Characterization and Application of Nanomaterials 2026, 9(2), 11764.
https://doi.org/10.24294/can11764

Article

Increasing the photocatalytic efficiency and electro-optical properties of titanium dioxide nanolayers doped with copper, silver and gold elements

Ali Asghar Khakpoor

Department of Physics, Central Tehran Branch, Islamic Azad University, Tehran 1955847781, Iran, ali.khakpoor@iauctb.ac.ir

CITATION

Khakpoor A A. Increasing the photocatalytic efficiency and electro-optical properties of titanium dioxide nanolayers doped with copper, silver and gold elements. Characterization and Application of Nanomaterials. 2026; 9(2): 11764. https://doi.org/10.24294/can11764

ARTICLE INFO

Received: 23 May 2026
Accepted: 25 May 2026
Available online: 16 June 2026

Abstract: To improve the photocatalytic activity of titanium dioxide nanolayers, we used doping with gold, silver, and copper nanoparticles. The nanolayers were prepared by the pulsed laser deposition (PLD) method. The surface morphology of the nanolayers was investigated using scanning electron microscopy (SEM), and the roughness and surface properties of the samples were measured using atomic force microscopy (AFM). X-ray diffraction (XRD) was used to characterize the crystal structure of the nanolayers. Also, the absorption spectra of the nanolayers were measured using a UV-Visible spectrophotometer. Their absorption and band gap changes were investigated and compared. A high increase in the absorption rate of nanolayers, especially compared to previous studies, was observed in the obtained results. The photocatalytic activity of the nanolayers was analyzed using the ISO-10678:2010 method for photonic efficiency, and the effect of doped elements in the structure of the nanolayers was studied. The results showed that doping titanium dioxide with metallic elements such as copper, silver, and gold significantly improves the photonic efficiency of nanolayers.

Keywords: titanium dioxide; pulsed laser deposition; nanoparticles; absorption efficiency; photonic efficiency.

1. Introduction

More than 2000 semiconductor materials have now been identified by researchers, most of which are oxides, sulfides, or nitrides based on transition metals [1–3]. Titanium dioxide remains one of the most promising semiconductor materials because of its high efficiency, low cost, chemical inertness, eco-friendly nature and Photo-stability [4,5].

Improving the electro-optical properties and increasing the efficiency of photocatalytic activity of photocatalytic materials and thin films is a hot topic for many researchers [6]. In a photocatalytic reaction in a semiconductor, upon irradiation with light, electrons in the valence band gain the energy required to be excited and jump to the conduction band, creating an electron-hole pair in the conduction and valence bands, respectively [7–16]. The electron-hole pair produced by the light migrates to the surface of the semiconductor material and participates in the photocatalytic reactions in the degradation of pollutants [17–21]. It should also be noted that the light absorption range of semiconductor materials is the visible light region up to a wavelength of 700 nm, making them very suitable for absorbing radiant energy from sunlight.

Doping nanolayers with elements that accelerate charge transfer reactions and also reduce the electron-hole pair recombination process is one way to increase the efficiency of photocatalytic activity, which can also lead to improvement of their

electro-optical properties. Titanium dioxide has also been and is the target of many researchers as a photocatalytic material whose photocatalytic activity is mainly in the ultraviolet radiation range [22–24].

Many efforts have been focused on reducing the optical band gap of titanium dioxide in order to improve its electro-optical properties. Therefore, doping of titanium dioxide nanolayers with various metal nanoparticles and their effect on electro-optical properties and photocatalytic activity have been investigated and studied [25–28]. Doping titanium dioxide with metal ions leads to a significant increase in photocatalytic activity, especially when it is doped with silver and copper, which has attracted considerable attention [26–28].

Varieties of nanocomposite semiconductor materials have been synthesized in recent years to improve the selectivity and efficiency of photocatalytic processes. One of the main concerns in photocatalytic activity is to improve their absorption coefficient. Therefore, doping different metal nanoparticles of different sizes, each of which absorbs different wavelengths of incident light, is one way to achieve this goal. For example, the effect of silver nanoparticles on increasing the absorption coefficient of TiO_2 thin films can be mentioned [29–34]. Another study investigated the effects of doping titanium dioxide nanolayers with copper nanoparticles, which led to a significant increase in the absorption coefficient [35]. It is also possible to mention a study that investigated the effect of gold nanoparticles on increasing the absorption coefficient of titanium dioxide nanolayers [36,37].

Also, many studies have investigated ways to enhance in photocatalytic activity of thin titanium dioxide layers. One of these studies is the high photocatalytic activity and degradation of methyl orange under UV irradiation using silver-doped titanium multilayer membranes by A. Alem and the other is the surface degradation of TiO_2 thin films modified with silver nanoparticles under sunlight irradiation by Ibrahim H.M.M and also the enhancement of photocatalytic activity of TiO_2 on Ag substrate by Nyamukamba et al. [38–40]. Also, the author has previously conducted studies on titanium dioxide nanolayers deposited on copper and silver nanolayers as well as on copper and silver nanoclusters [41–46]. Many studies have been conducted in this field and some interesting research can be found in these references [47–50].

In this research, the aim is to increase the photocatalytic efficiency of titanium dioxide nanolayers as well as titanium dioxide nanolayers doped with copper, silver and gold and compare them. In addition, the effect of UV irradiation time on the photocatalytic efficiency has been investigated.

2. Materials and methods

2.1. Experimental methods

Each time, one of the samples is placed in the vacuum chamber as a target. The vacuum system was pumped from 10^{-6} Torr to a final pressure of 2×10^{-5} Torr. The substrates were made of quartz and cut into 10×10 mm pieces. Pulsed laser deposition (PLD) in the presence of argon gas was used to deposit pure and doped TiO_2 nanolayers. A KrF laser (248 nm wavelength, 2 J/cm^2 energy density, 7.5×10^{-3}

Torr argon gas, 25 ℃ substrate temperature, 5 cm target-substrate distance, 10 Hz pulse repetition rate, and 10,000 pulses) was used to grow TiO_2 nanolayers. Since the energy required to detach atoms from the target surface is provided by momentum transfer, the impurity or purity of the target is not important. The titanium dioxide powder that was used in this work was prepared by Kimia Eksir Company. Copper, silver, and gold powders were used as impurities. The dopant is added to titanium dioxide powder in 5% the weight, as **Table 1** and four different samples were prepared, and were initially completely cleaned of contaminants.

Table 1. Weight percentage of dopant in different samples.

Sample	Titanium dioxide (%)	Dopant (%)
S_1	100	0
S_2	95	Cu (5%)
S_3	95	Ag (5%)
S_4	95	Au (5%)

Then, nanolayers were deposited by sputtering and their thickness was measured during the deposition process. The nanolayers were coated on a quartz substrate with a thickness of 350 ± 35 nm.

2.2. Analysis of samples

The X-ray diffraction patterns of the nanolayers were prepared using a PHILIPS model PW1730 (Cukα with a wavelength of 0.154056 nm). The surface morphology of the nanolayers was studied using a Hitachi S-4160 field emission electron microscope (FE-SEM). The roughness and surface properties of the samples were measured using image recording using the contact mode of the Auto Probe CP atomic force microscope (AFM) manufactured by Park Scientific Instruments, USA. The absorption spectra of the layers in the range of 200 to 1100 nm were measured using an Ocean optics HR4000 UV-Vis spectrometer.

2.3. Photocatalytic activity

ISO-10678:2010 is a standard for measuring and comparing the photocatalytic activity of different nanolayers. This is done by measuring the photonic efficiency of the nanolayers. This photonic efficiency is equal to the percentage of photons irradiated per unit area that participate in photocatalytic activity per unit time, and in this standard, methylene blue is used as the dye solution and ultraviolet radiation with a wavelength of 365 nm is used [45,46].

Dye solution was added to a cuvette containing a nanolayer with a 1 cm^2 area. To establish an adsorption and desorption equilibrium, the cuvette was placed in the dark for 24 h, and then it was exposed to ultraviolet light at different times. The radiation source was capable of providing a radiation intensity (E) of 14 W/m^2 at a distance of 7 cm from the surface of the samples. A UV intensity measuring device (UV-340A) manufactured by LUTRON, Taiwan, was used to measure the radiation intensity of the source. The photonic efficiency can be obtained as follows:

$$\zeta_{MB} = [\ (\Delta A_\lambda\ V) / (\Delta t\ A\ \varepsilon\ d\ \lambda_{max}\ E)]\ \times 100 \quad (1)$$

In this equation, λ_{max} and E are the maximum wavelength and the source intensity of radiation, respectively, where E is equal to 14 W/m^2. Also, ΔA_λ, Δt, V, A, d and ε are the changes in methylene blue absorption, irradiation time, volume of solution under irradiation, active surface area, cuvette irradiation length and methylene blue offset coefficient, respectively, which (ε_{664} nm = 7402.8 m^2/mol). The device used for UV-visible spectroscopy measurements is a Varian spectrometer (model Cary 100 Bio).

3. Results and discussion

3.1. XRD analysis

Figure 1 shows XRD patterns of samples.

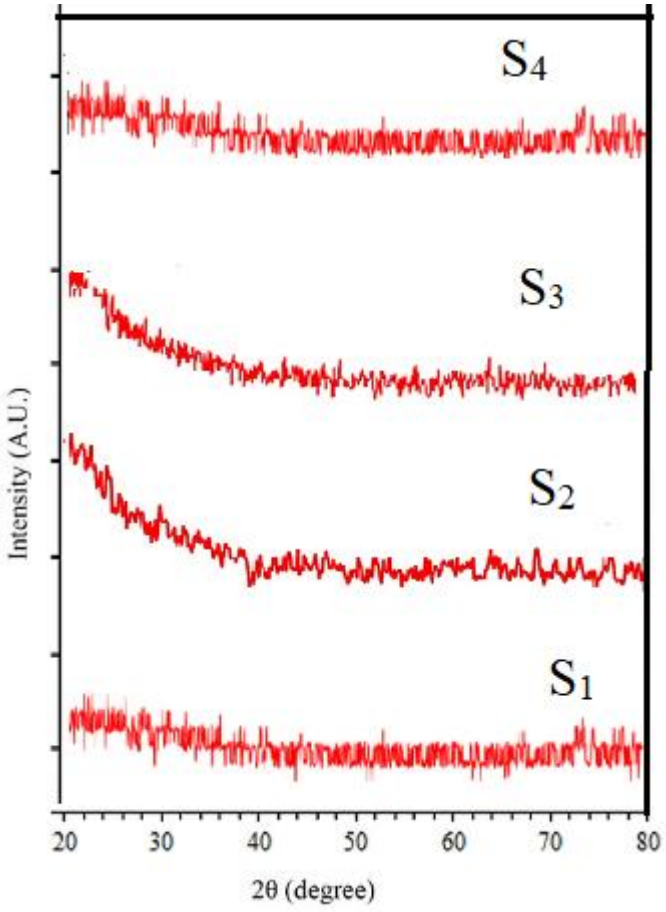

Figure 1. XRD patterns of samples.

Figure 1 shows that all samples, both pure titanium dioxide nanolayers and doped nanolayers, are completely amorphous and lack a crystalline structure. This is in complete agreement with the characteristics of titanium dioxide nanolayers that have not been subjected to heat treatment, and we know that with heat treatment at a temperature of close to 400 ℃, the phase transition process from amorphous to anatase begins and is completed at higher temperatures.

Based on XRD, which shows broad peaks indicating an amorphous nature, it can be concluded that the impurities are present in the form of highly dispersed metal nanoclusters and substitution ions embedded in the TiO_2 structure, which is consistent with the observed electronic behavior.

3.2. Surface morphology of nanolayer

Figures 2 and **3** show the FE-SEM images of the samples, in which we can see that the particle size in all samples is in the range of 10 to 300 nm. However, the particle size in each sample is slightly different. This difference in size could be due to the impurity elements and the difference in their particle size, which causes the formation and orientation of particles with different sizes. Image of sample S_1 (image a) shows a nanolayer with a rough surface and a compact structure. The surface morphology of sample S_2 (image b) shows a rougher and more compact structure with a slightly larger particle size than S_1. The particle size and surface roughness of the nanolayers in sample S_3 (image c) further increase and become more compact, and finally reach their maximum in sample S_4 (image d).

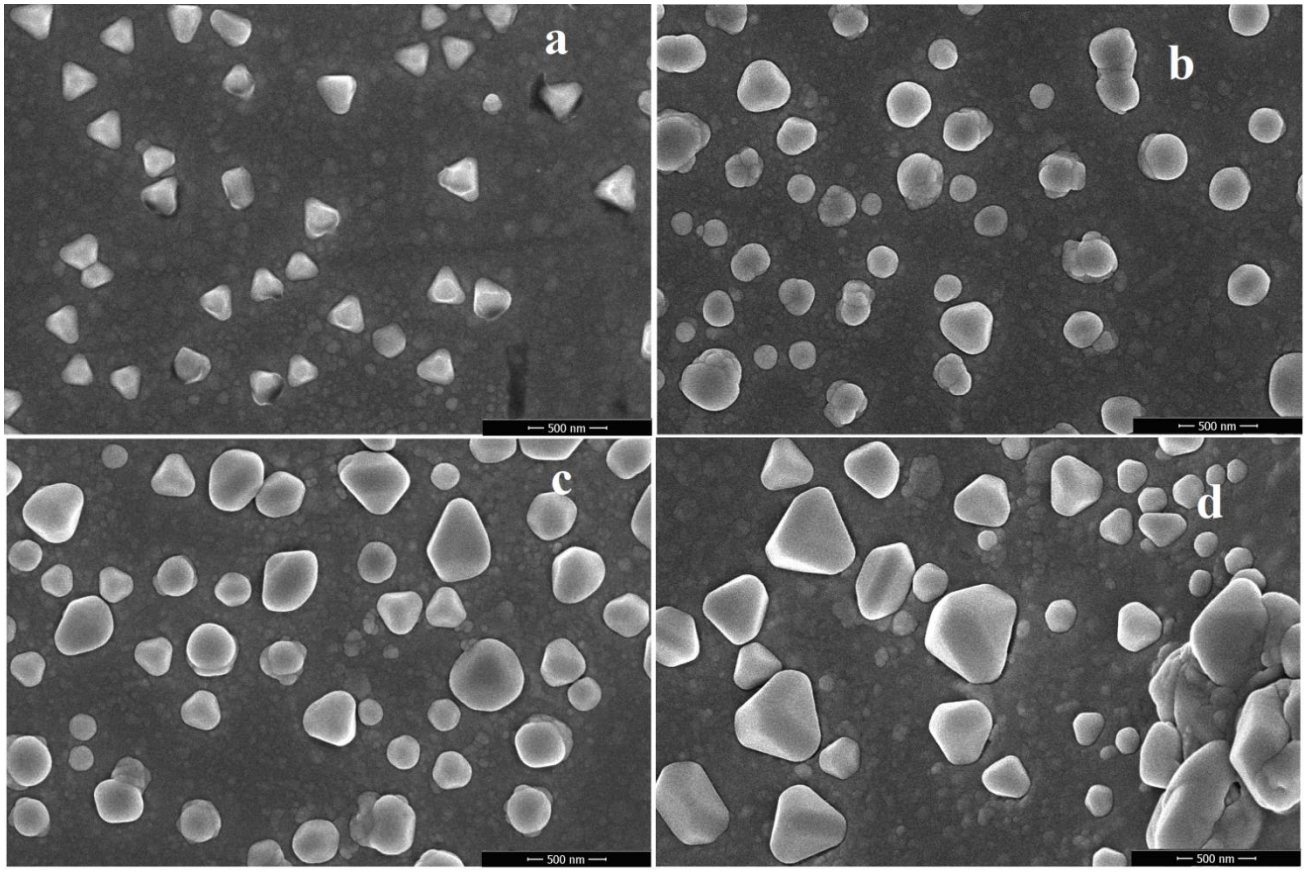

Figure 2. FE-SEM images of samples at 500 nm magnification: (**a**) S1, (**b**) S2, (**c**) S3, and (**d**) S4.

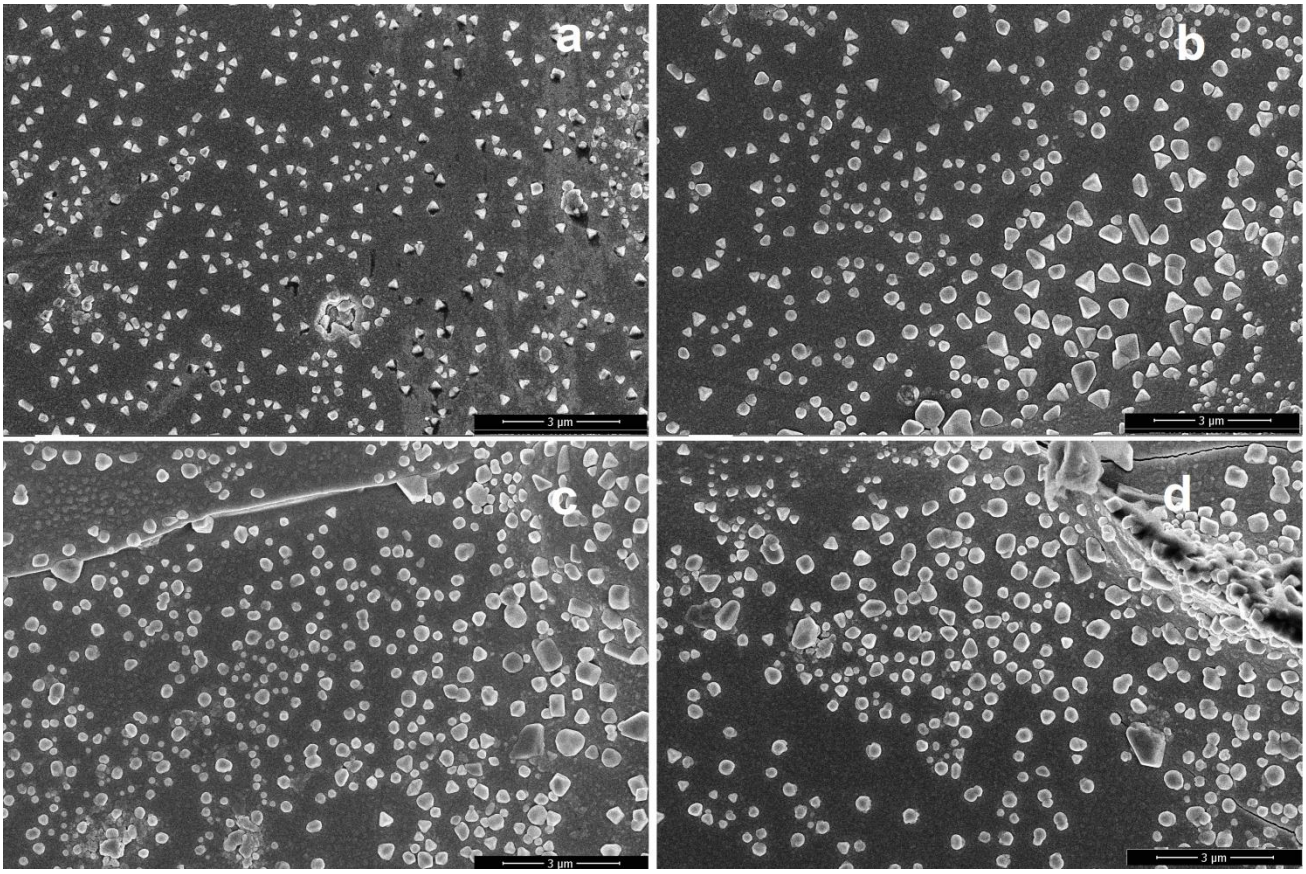

Figure 3. FE-SEM images of samples at 3 µm magnification: (**a**) S1, (**b**) S2, (**c**) S3, and (**d**) S4.

3.3. AFM analysis

Figure 4 shows the AFM analysis of the samples. The AFM analysis shows an increase in roughness and formation of pores on the surface of the nanolayer in the presence of dopants. This roughness is higher in samples S_2, S_3 and S_4 than in sample S_1. The information on the average linear roughness of the samples obtained from AFM analysis is shown in **Table 2**.

Table 2. Linear roughness average (Ra) of all samples obtained from AFM analysis.

Sample	R_a (nm)
S_1	0.309
S_2	0.408
S_3	0.491
S_4	0.527

AFM images and linear surface roughness results show that the surface roughness of the nanolayers increased with the presence of metal contaminants such as copper, silver, and gold.

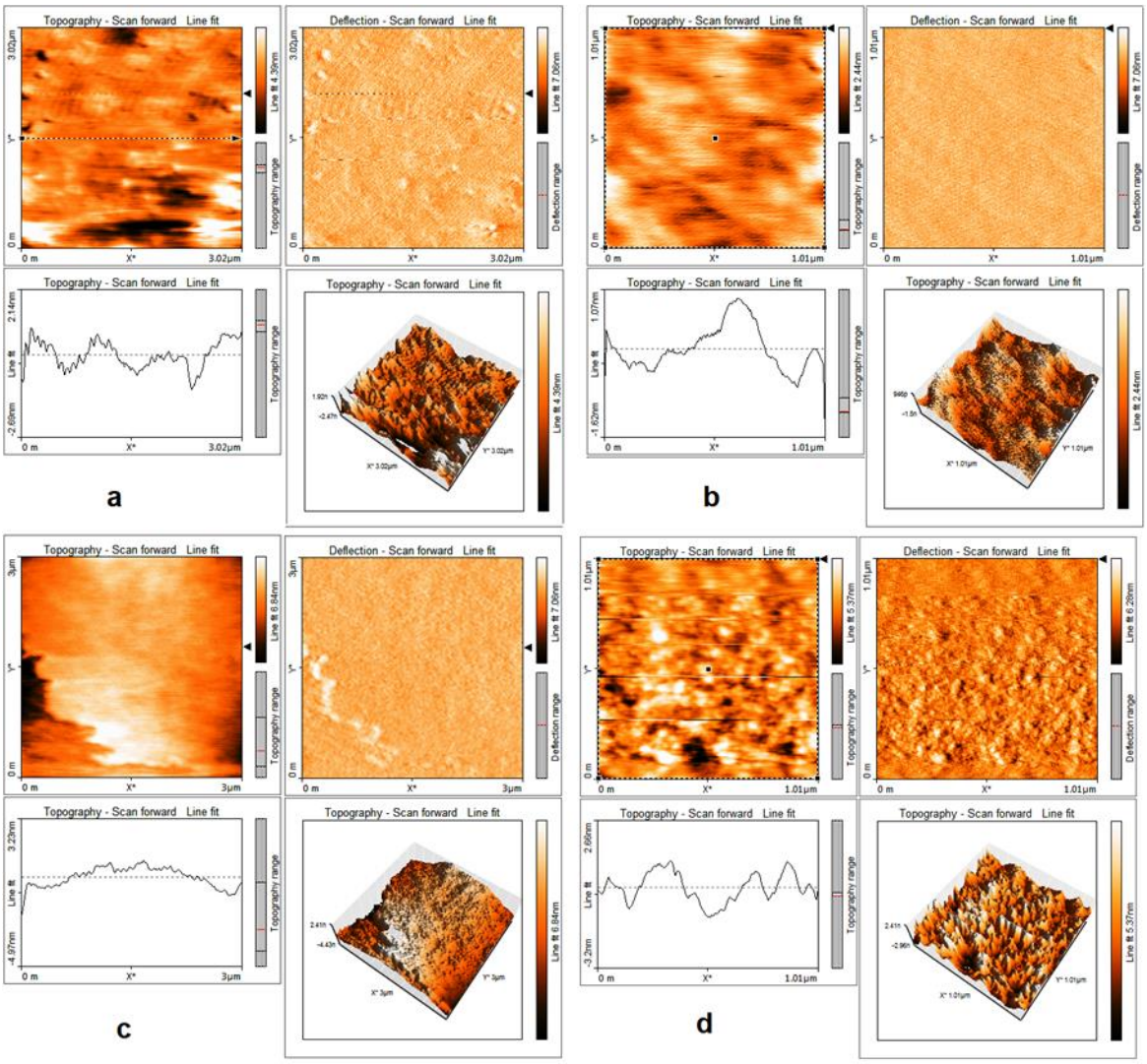

Figure 4. 2D, 3D images and linear topography of AFM analysis: (**a**) S_1, (**b**) S_2, (**c**) S_3, and (**d**) S_4

3.4. Absorption spectra of the samples

Figure 5 shows the UV-Vis spectra of pure and doped titanium dioxide nanolayers. As can be seen, the absorption coefficient of all samples in the ultraviolet range is high. However, in all samples, as the wavelength increases and approaches the visible region, it decreases sharply, and in the visible region, the absorption is very low and the transmission of the nanolayers is high. The absorption of the samples in the visible region is slightly different, which is due to the doped elements. So, in samples S_3 and S_4, we observe a higher absorption rate, which is due to the presence of gold and silver in the structure of the layers. In addition, in samples S_2 to S_4, several wide absorption bands are observed, and the presence of these absorption bands is more noticeable in sample S_3. The reason for this increase is the vibrations of surface plasmons caused by the presence of copper, silver, and gold nanoparticles on the surface of the nanolayers, which have been mentioned in some articles [43,45,46]. The location, number, and width of these absorption bands vary due to differences in doped elements.

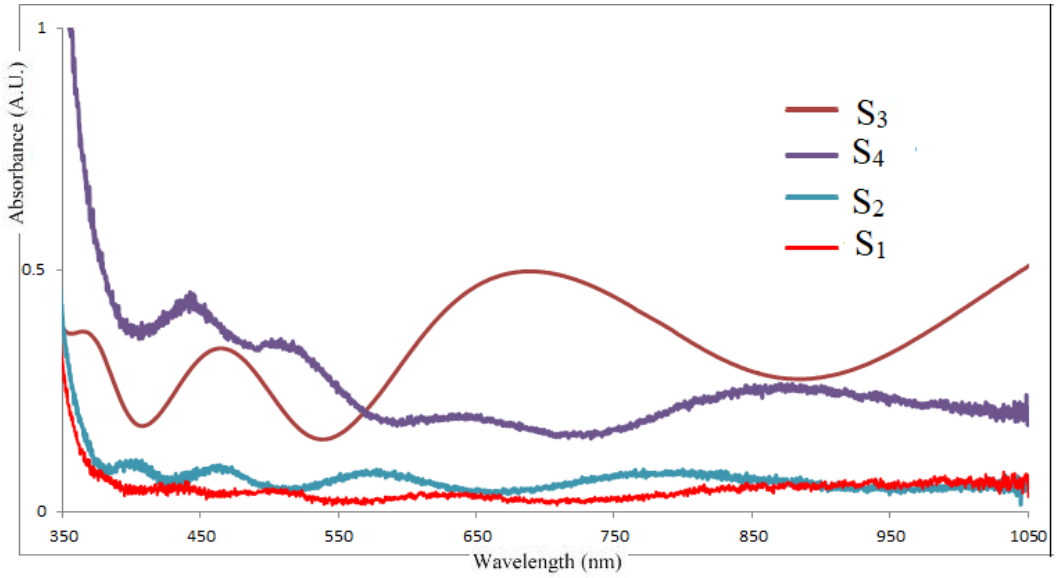

Figure 5. The UV-Vis spectra of samples.

The optical constants of nanolayers, such as the optical absorption coefficient α, can be calculated in various ways. One of the simplest and most popular laboratory methods is to use their absorption and transmission spectra, which are defined as follows, depending on the thickness of the nanolayer:

$$\alpha = \frac{2.303}{t} \log\left(\frac{I_0}{I}\right) \quad (2)$$

In this equation, I_0, I and t are the intensity of the light incident on the layer, the intensity of the transmitted light and, the layer thickness, respectively. The absorbance edge (E_g) of titanium dioxide nanolayers is shifted to vision region using the Tauc's equation [51]:

$$(\alpha h\nu)^2 = k(h\nu - Eg)^n \quad (3)$$

Where $h\nu$ is the photon energy and k and n are constants, with the value of n being 1 or 3 for semiconductors with direct and indirect energy band gaps, respectively. When Equation (2) is equal to zero, the energy band gap will be equal to the energy of the photon shown. Therefore, the energy band gap of the nanolayer can be calculated from the Tauc's curves. **Figure 6** shows the Tauc's curves for the samples. Where the curves become linear, the direct energy band gaps of these semiconductors can be calculated. The direct energy band gap values of the samples were calculated and listed with an uncertainty of 0.16 eV in **Table 3**.

Table 3. The direct energy band gap of samples.

Sample	**S_1**	**S_2**	**S_3**	**S_4**
E_g (eV)	3.19	3.12	2.97	2.86

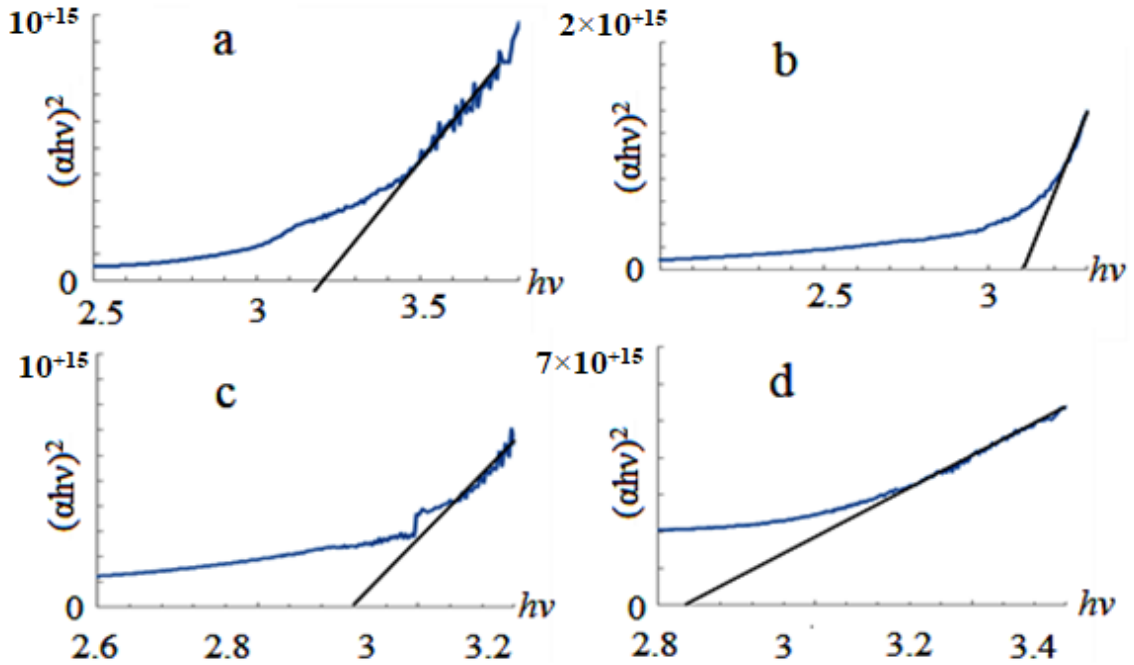

Figure 6. The curves of Tauc's equation of samples.

The reason for the band gap reduction in the presence of metal impurities could be the presence of a metal Fermi level in the band gap of titanium dioxide, which has been reported in some papers [33]. For example, the band gap reduction (from 3.19 eV for S_1 to 2.86 eV for S_4 in **Table 3**) is due to mid-gap defect states originating from localized d-orbitals of the noble metal dopants. **Figure 7** shows a schematic diagram of the energy band structure, showing the interband states derived from the valence band (VB), conduction band (CB), d-orbitals, and band gap for pure and doped titanium dioxide.

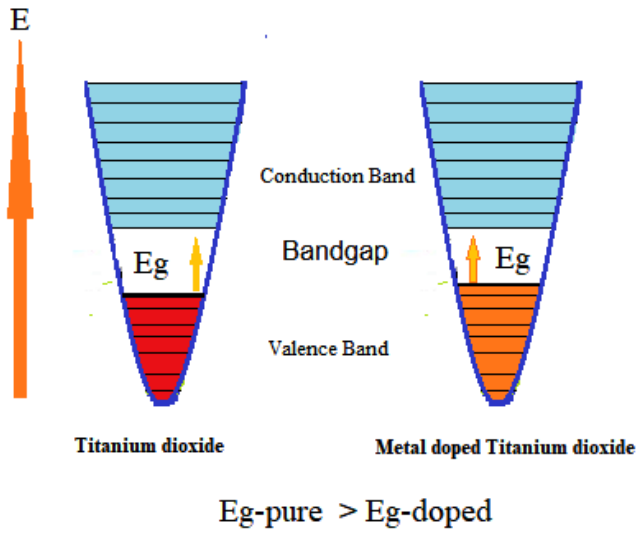

Figure 7. Schematic diagram of the energy band structure of pure and doped titanium dioxide.

3.5. Photocatalytic test

The initial concentration of the Methylene Blue (MB) solution used for all degradation experiments is 2 mL of a 10 μM solution. Each sample with an active surface area of 1 cm^2 was placed at the bottom of a cuvette. Then, 2 mL of a 10 μM methylene blue solution was added to each cuvette. To balance adsorption and desorption between the surface of the layer and the solution, we placed cuvettes containing the samples and the methylene blue solution in the dark for 24 h. A control sample in which the cuvette lacked the nanolayer was also examined. After 24 h, the solution was exposed to UV radiation and samples were taken at 30, 60, 90, and 120 min after the start of irradiation. Spot absorption was measured by ultraviolet-visible spectroscopy at a wavelength of 664 nm. The results obtained are shown in **Table 4**.

Table 4. Spot absorption of samples was measured by ultraviolet-visible spectroscopy.

Sample	$A_{30\ min}$	$A_{60\ min}$	$A_{90\ min}$	$A_{120\ min}$
Control sample	0.5391	0.5388	0.5386	0.5385
S_1	0.4317	0.3934	0.3413	0.2925
S_2	0.4174	0.3594	0.3202	0.2747
S_3	0.4047	0.3517	0.3188	0.2691
S_4	0.4012	0.3474	0.3106	0.2670

The changes in the absorption coefficient of the samples exposed to ultraviolet radiation after 30, 60, 90, and 120 min from the start of radiation were calculated using **Table 4**, and the results are given in **Table 5**. **Figure 8** also shows the information obtained in **Table 4** for the changes in the absorption coefficient.

Table 6 shows the results of the photonic efficiency under UV irradiation after 30, 60, 90 and 120 min, which are calculated based on the information in **Table 5**. **Figure 9** shows the changes in the photonic efficiency of the samples based on the UV irradiation time.

Table 5. Changes in the absorption coefficient of samples depending on the time of ultraviolet irradiation.

Sample	$\Delta A_{30\ min}$	$\Delta A_{60\ min}$	$\Delta A_{90\ min}$	$\Delta A_{120\ min}$
S_1	0.1074	0.1454	0.1973	0.2460
S_2	0.1217	0.1794	0.2184	0.2638
S_3	0.1344	0.1871	0.2198	0.2694
S_4	0.1379	0.1914	0.2280	0.2715

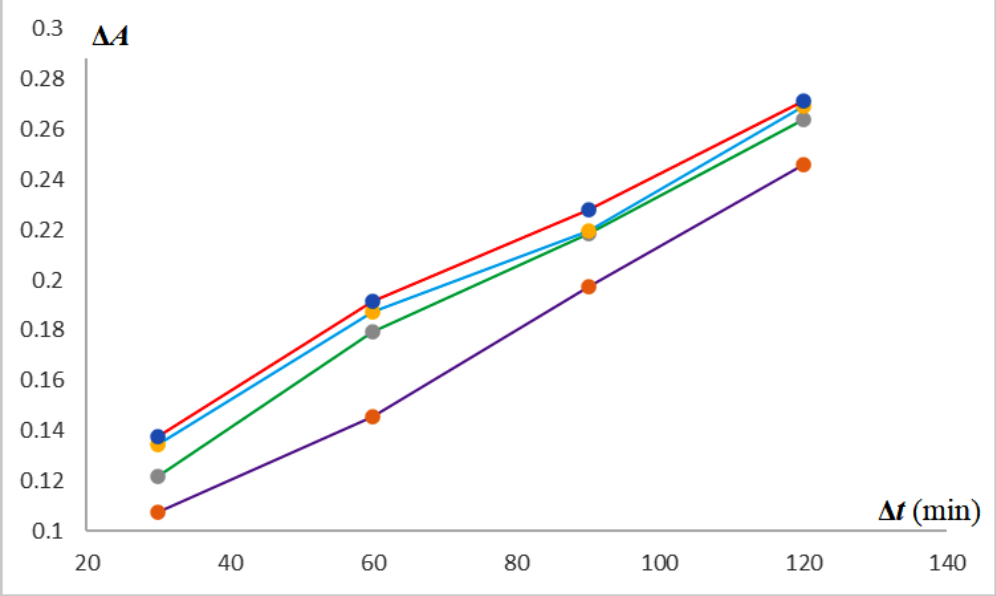

Figure 8. Graph of changes in the absorption coefficient of samples depending on the time of ultraviolet irradiation.

Table 6. The photonic efficiency under UV irradiation after 30, 60, 90 and 120 min.

Sample	$\zeta_{MB\text{-}30\ min}$ (%)	$\zeta_{MB\text{-}60\ min}$ (%)	$\zeta_{MB\text{-}90\ min}$ (%)	$\zeta_{MB\text{-}120\ min}$ (%)
S_1	19.37	13.11	11.86	11.09
S_2	21.95	16.18	13.13	11.89
S_3	24.24	16.87	13.21	12.15
S_4	24.88	17.26	13.71	12.24

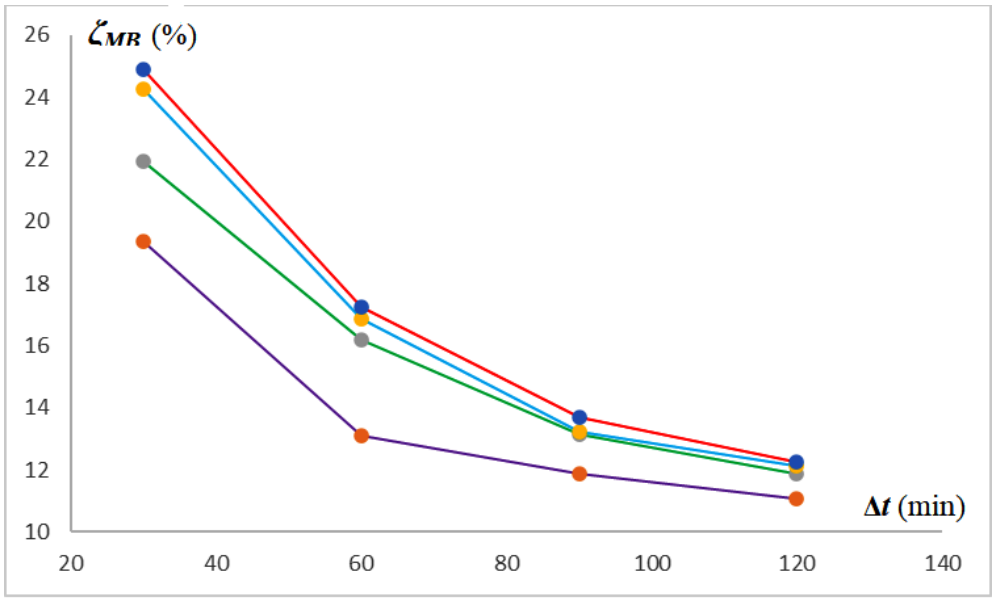

Figure 9. The changes in the photonic efficiency of the samples depending on the time of ultraviolet irradiation.

Doping of metallic elements copper, silver and gold in the structure of titanium dioxide nanolayers due to the difference in particle size increases the surface roughness of the nanolayers, which leads to an increase in surface active sites in

photocatalytic activity and the surface charge carrier transfer ratio. Therefore, the absorption coefficient and photonic efficiency of the nanolayers increase [22]. In **Figure 9**, the photonic efficiency has increased significantly due to the doping of these metallic elements. Although the type of doped element does not make a significant difference, the highest efficiency is related to the nanolayer doped with gold, followed by silver. It can be seen from **Figure 6** that the longer the samples are exposed to UV radiation, the more the photonic efficiency decreases. This occurs for all samples, but with slightly different attenuation coefficients and the photonic efficiency decreases almost exponentially with time. This effect is due to the recombination of electron-hole pairs and the reduction of photocatalytically active sites, which is an exponential function of time [45,46].

4. Conclusion

In the presence of metallic contaminants such as copper, silver, and gold, the surface roughness of the nanolayers increased, which increased the number of surface active sites on the photocatalyst surface, resulting in an increase in the photonic efficiency and absorption coefficient of the samples. The absorption coefficients of pure titanium dioxide nanolayers and those doped with copper, silver, and gold nanoparticles sputtered onto quartz substrates are all in the ultraviolet range and above. However, doping these metal elements in the titanium dioxide nanolayer structure causes a shift in the absorption spectrum and also the absorption edge of the titanium dioxide nanolayer towards the optical region of the electromagnetic spectrum. The magnitude of this shift in the absorption spectrum and absorption edge in the gold-doped titanium dioxide nanolayer is slightly greater than that in the silver-doped titanium dioxide nanolayer, and the silver-doped titanium dioxide nanolayer is slightly greater than that in the copper-doped titanium dioxide nanolayer, which can be attributed to the change in the size of the doped elements and a slight difference in the location of the Fermi level of these three elements.

Titanium dioxide nanolayers doped with copper, silver, and gold elements also have better photocatalytic activity and higher photonic efficiency, which is due to the difference in the size of the impurities, which creates a larger effective surface area and increases the number of active sites in the photocatalytic activity, and the second effect is to reduce the electron-hole pair recombination process in the photocatalytic activity by trapping surface electrons by the metal. In other words, while the metal species increase the number of active sites in the photocatalytic activity, they also act as electron trapping sites. By spatially separating the light-generated electrons from the holes, this trapping effectively reduces the rate of harmful electron-hole recombination, thereby maximizing the number of carriers available for the photocatalytic reaction. The slight difference observed in the doped samples is due to this difference in the location of their Fermi level, which is located in the band gap of titanium dioxide. Therefore, titanium dioxide nanolayers doped with gold, silver and copper elements, respectively and with a slight difference, have the highest photon efficiency in the photocatalytic activity.

Acknowledgments: The author would like to thank Islamic Azad University Central Tehran Branch, (CT.C.IAU) for helpful protections.

Conflict of interest: The author declare they have no competing interests.

References

1. Liang M, Shao X, Cho Y, et al. Effective charge separation in a dual-single-atom photocatalyst for sacrificial agent-free H2 evolution. ACS Sustainable Chemistry & Engineering. 2024; 12(16): 6122–6131. https://doi.org/10.1021/acssuschemeng.3c07119
2. Fu F, Liu Y, Liu M, et al. Non-noble metal single-molecule photocatalysts for the overall photosynthesis of hydrogen peroxide. Journal of the American Chemical Society. 2024. https://doi.org/10.1021/jacs.4c09445
3. Ponnumsamy VK, Al-Hazmi HE, Shobana S, et al. A review on homogeneous and heterogeneous catalytic microalgal lipid extraction and transesterification for biofuel production. Chinese Journal of Catalysis. 2024; 59: 97–117. https://doi.org/10.1016/S1872-2067(23)64626-1
4. Leaverand KD, Chapman BN. Thin Films. London, England: The Wykeham Science Press; 1971.
5. Mehrzad A, Khakpoor AA, Mortazavi S, et al. Synthesis and photocatalytic activity of TiO_2 monodisperse nanoparticles at low temperatures. Journal of Nanoelectronics and Optoelectronics. 2018; 13(2): 156–162. https://doi.org/10.1166/jno.2018.2226
6. Deng Y, Chen M, Chen G, et al. Visible–ultraviolet upconversion carbon quantum dots for enhancement of the photocatalytic activity of titanium dioxide. ACS Omega. 2021; 6(6): 4247–4254. https://doi.org/10.1021/acsomega.0c05182
7. Dong Y, Zhang W, Hu Z, et al. Advancing CO2 to CH4 conversion: The pivotal role of RuCu alloy in crystalline red phosphorus photocatalysis. Applied Catalysis B: Environment and Energy. 2024; 357: 124347. https://doi.org/10.1016/j.apcatb.2024.124347
8. Yadav A, Singal S, Kumar J, et al. Sonochemically synthesized porous V2CTX MXene/red-black phosphorus composite: A promising electrode for supercapacitors. Journal of Energy Storage. 2024; 79: 110155. https://doi.org/10.1016/j.est.2023.110155
9. Li T, Guan C, Xu L, et al. Facile synthesis of MoS2@red phosphorus heterojunction for synergistically photodynamic and photothermal therapy of renal cell carcinoma. Colloids and Surfaces B: Biointerfaces. 2024; 241: 114031. https://doi.org/10.1016/j.colsurfb.2024.114031
10. Qasim M, Liu M, Guo L. Z-scheme P doped-g-C3N4/Fe2P/red-P ternary composite enables efficient two-electron photocatalytic pure water splitting. Catalysis Today. 2023; 409: 117–129. https://doi.org/10.1016/j.cattod.2022.05.007
11. Singh S, Kansal SK. Enhanced performance of dual-functional ZIF-8/red phosphorus photocatalysts for concurrent degradation of organic dyes and hydrogen generation under natural solar light irradiation. Chemical Communications. 2024; 60: 10970–10973. https://doi.org/10.1039/d4cc02644f
12. Liu M, Guan L, Wen Y, et al. Rice husk biochar mediated red phosphorus for photocatalysis and photothermal removal of E. coli. Food Chemistry. 2023; 410: 135455. https://doi.org/10.1016/j.foodchem.2023.135455
13. Duan Y, Li R, Liu Q, et al. Elemental phosphorus for recent sustainable processes: Rules and strategies in preparation and applications. Green Chemistry. 2022; 24: 3475–3501. https://doi.org/10.1039/d2gc00727d
14. Khiar H, Barka N, Puga A. Metal phosphates for the design of advanced heterogeneous photocatalysts. Coordination Chemistry Reviews. 2024; 510: 215814. https://doi.org/10.1016/j.ccr.2024.215814
15. Zhao F, Miao H, Fan J, et al. Fabrication of S-scheme FeCoS2/Red phosphorus heterojunction for efficient photocatalytic H2 evolution. Colloids and Surfaces A: Physicochemical and Engineering Aspects. 2023; 676: 132316. https://doi.org/10.1016/j.colsurfa.2023.132316
16. Singh S, Kansal SK. Recent progress in red phosphorus-based photocatalysts for photocatalytic water remediation and hydrogen production. Applied Materials Today. 2022; 26: 101345. https://doi.org/10.1016/j.apmt.2021.101345
17. Wang Y, Li X, Mei T, et al. Surface sulphur vacancies of CdS/MIL-68(In)-NH2 for boosting visible-light photocatalytic hydrogen evolution. Inorganic Chemistry Communications. 2024; 168: 112987. https://doi.org/10.1016/j.inoche.2024.112987
18. Zhang Y, Zhou Y, Li MMJ, et al. Surface site design in photocatalytic carbon conversion applications. Coordination Chemistry Reviews. 2025; 529: 216459. https://doi.org/10.1016/j.ccr.2025.216459

19. Wei H, Wan R, Zhang Z, et al. Potential of two-dimensional AgAlP2Se6 monolayer for high-efficiency photocatalytic hydrogen production. Materials Science in Semiconductor Processing. 2025; 186: 109040. https://doi.org/10.1016/j.mssp.2024.109040
20. Masekela D, Kganyakgo LK, Modibane KD, et al. Green synthesis and enhanced photocatalytic performance of Co-doped CuO nanoparticles for efficient degradation of synthetic dyes and water splitting. Results in Chemistry. 2025; 13: 101971. https://doi.org/10.1016/j.rechem.2024.101971
21. Liu N, Su Y, Zheng S, et al. Impact of ligand on layered sulfur nanosheets/g-C3N4 nanocomposite for photocatalytic degradation. Journal of Photochemistry and Photobiology A: Chemistry. 2025; 463: 116274. https://doi.org/10.1016/j.jphotochem.2025.116274
22. Zaleska A. Doped-TiO_2: a review. Recent Patents on Engineering. 2008; 2: 157–164. https://doi.org/10.2174/187221208786306289
23. Lee YC, Hong YP, Lee HY, et al. Photocatalysis and hydrophilicity of doped TiO2 thin films. Journal of Colloid and Interface Science. 2003; 267: 127–131. https://doi.org/10.1016/s0021-9797(03)00603-9
24. Domaradzki J, Kaczmarek D, Prociow EL, et al. Optical and electrical properties of TiO_2 doped with Tb and Pd. Materials Science Poland. 2008; 26: 143–147.
25. Rahman MM, Krishna KM, Soga T, et al. Optical properties and X-ray photoelectron spectroscopic study of pure and Pb doped TiO2 thin films. Journal of Physics and Chemistry of Solids. 1999; 60: 201–210. https://doi.org/10.1016/S0022-3697(98)00264-9
26. Mardare D, Tasca M, Delibas M, et al. On the structural properties and optical transmittance of TiO2 r.f. sputtered thin films. Applied Surface Science. 2000; 156: 200–206. https://doi.org/10.1016/S0169-4332(99)00508-5
27. Sonawane RS, Dongare MK. Sol–gel synthesis of Au/TiO_2 thin films for photocatalytic degradation of phenol in sunlight. Journal of Molecular Catalysis. 2006; 243: 68–76. https://doi.org/10.1016/j.molcata.2005.07.043
28. Wang SF, Hsu YF, Lee YS. Microstructural evolution and optical properties of doped TiO2 films prepared by RF magnetron sputtering. Ceramics International. 2006; 32: 121–125. https://doi.org/10.1016/j.ceramint.2005.01.010
29. He J, Ichinose I, Kunitake T, et al. In situ synthesis of noble metal nanoparticles in ultrathin TiO_2−gel films by a combination of ion-exchange and reduction processes. Langmuir. 2002; 18(25): 10005–10010. https://doi.org/10.1021/la0260584
30. He C, Xiong Y, Chen J, et al. Photoelectrochemical performance of Ag–TiO_2/ITO film and photoelectrocatalytic activity towards the oxidation of organic pollutants. Journal of Photochemistry and Photobiology A: Chemistry. 2003; 157(1): 71–79. https://doi.org/10.1016/S1010-6030(03)00080-7
31. Arabatzis IM, Stergiopoulos T, Bernard MC, et al. Silver-modified titanium dioxide thin films for efficient photodegradation of methyl orange. Applied Catalysis B: Environmental. 2003; 42(2): 187–201. https://doi.org/10.1016/S0926-3373(02)00233-3
32. Szabó-Bárdos E, Czili H, Horváth A. Photocatalytic oxidation of oxalic acid enhanced by silver deposition on a TiO2 surface. Journal of Photochemistry and Photobiology A: Chemistry. 2003; 154(2–3): 195–201. https://doi.org/10.1016/S1010-6030(02)00330-1
33. Yu J, Xiong J, Cheng B, et al. Fabrication and characterization of Ag–TiO2 multiphase nanocomposite thin films with enhanced photocatalytic activity. Applied Catalysis B: Environmental. 2005; 60(3–4): 211–221. https://doi.org/10.1016/j.apcatb.2005.03.009
34. Su W, Wei SS, Hu SQ, et al. Preparation of TiO_2/Ag colloids with ultraviolet resistance and antibacterial property using short chain polyethylene glycol. Journal of Hazardous Materials. 2009; 172(2–3): 716–720. https://doi.org/10.1016/j.jhazmat.2009.07.056
35. Men Y, Kolb G, Zapf R, et al. Selective methanation of carbon monoxide in hydrogen-rich reformate using microstructured reactor. Chemistry Letters. 2009; 38(8): 824–825. https://doi.org/10.1246/cl.2009.824
36. Han JB, Ding S, Chen DJ, et al. Microstructure and percolation threshold characteristics of reactive sputtered Au–TiO_2 granular composite films. Journal of Non-Crystalline Solids. 2006; 325(5): 386–389. https://doi.org/10.1016/j.jnoncrysol.2006.01.004
37. Tom RT, Nair AS, Singh N, et al. Freely dispersible Au@TiO_2, Au@ZrO_2, Ag@TiO_2, and Ag@ZrO_2 core−shell nanoparticles: One-step synthesis, characterization, spectroscopy, and optical limiting properties. Langmuir. 2003; 19(8): 3439–3445. https://doi.org/10.1021/la0266435

38. Alem A, Sarpoolaky H. The effect of silver doping on photocatalytic properties of titania multilayer membranes. Solid State Sciences. 2010; 12(8): 1469–1472. https://doi.org/10.1016/j.solidstatesciences.2010.06.009
39. Ibrahim HM. Photocatalytic degradation of methylene blue and inactivation of pathogenic bacteria using silver nanoparticles modified titanium dioxide thin films. World Journal of Microbiology and Biotechnology. 2015; 31: 1049–1060. https://doi.org/10.1007/s11274-015-1855-9
40. Nyamukamba P, Tichagwa L, Ngila JC, et al. Plasmonic metal decorated titanium dioxide thin films for enhanced photodegradation of organic contaminants. Journal of Photochemistry and Photobiology A: Chemistry. 2017; 343: 85–95. https://doi.org/10.1016/j.jphotochem.2017.04.014
41. Khakpoor AA, Borjian R, Hoseinzade M. Optical properties improvement TiO_2 thin films with adding the Au, Ag or Cu nanoparticles. International Materials Physics Journal. 2013; 1(2): 8–13.
42. Kavei G, Ahmadi K, Khakpoor AA. Oxide glasses doped with silver nanoparticles: properties and technologies. International Materials Physics Journal. 2013; 1(1): 40–46.
43. Mortazavi S, Khakpoor AA, Mehrzad A, et al. Study of the photocatalytic activity and hydrophilic properties in the titanium dioxide layer deposited on copper nanoclusters. Journal of Nanoelectronics and Optoelectronics. 2019; 14(2): 272–279. https://doi.org/10.1166/jno.2019.2490
44. Khakpoor AA, Ahmadi K, Kavei G. Formation of a titanium dioxide layer on Cu nanoclusters as a hydrophilic surface. Journal of Advanced Physics. 2017; 6(4): 573–578.
45. Mortazavi S, Khakpoor AA, Mehrzad A, et al. The formation and characterization of titanium dioxide layers deposited on copper middle nano-layer. Optical and Quantum Electronics. 2018; 50(11): 384. https://doi.org/10.1007/s11082-018-1648-0
46. Borazjani B, Khakpoor AA. High photocatalytic efficiency and hydrophilicity of titanium dioxide nanolayer deposited on silver intermediate nanolayer. Surfaces and Interfaces. 2025; 59: 105914. https://doi.org/10.1016/j.surfin.2025.105914
47. Peng X, Li J, Cao X, et al. Rational design of novel Ag-MoS2@COF ternary heterojunctions and their photocatalytic applications. Journal of Molecular Structure. 2025; 1328: 141395. https://doi.org/10.1016/j.molstruc.2025.141395
48. Chen X, Zhen C, Qiu J, et al. Modulating band alignment at the 3D metal/semiconductor interface of liquid metal-embraced semiconductor photoelectrodes for water splitting. Science China Materials. 2024; 67: 1804–1811. https://doi.org/10.1007/s40843-024-2929-6
49. Zheng D, Wang Q, Pan Z, et al. Poly(triazine imide) nanospheres with spatially exposed prismatic facets for photocatalytic overall water splitting. Science China Materials. 2024; 67: 1900–1906. https://doi.org/10.1007/s40843-023-2752-9
50. Bouziani M, Bouziani A, Zaari H, et al. Tuning the optical and photocatalytic properties of hexagonal boron nitride through Fe and Co doping: A DFT study. Computational and Theoretical Chemistry. 2025; 1245: 115095. https://doi.org/10.1016/j.comptc.2025.115095
51. Tauc J. Absorption edge and internal electric fields in amorphous semiconductors. Materials Research Bulletin. 1970; 5: 721–729. https://doi.org/10.1016/0025-5408(70)90112-1